Mesoscience & Nanotechnology
DOI: Article

# Thickness-dependent superconductivity in MoRe films studied by terahertz spectroscopy

E. S. Zhukova,[1] B. M. Nekrasov,[1] L. S. Kadyrov,[1] A. V. Melentev,[1] A. S. Shaimardanov,[1,2] A. G. Shishkin,[1,2,3] A. A. Golubov,[4] M. Yu. Kupriyanov,[2,5] B. P. Gorshunov,[1] and V. S. Stolyarov[1,2,3]

[1] *Moscow Institute of Physics and Technology (National Research University), 141700 Dolgoprudny, Russia*
[2] *National University of Science and Technology (MISIS), 119049 Moscow, Russia*
[3] *Dukhov Research Institute of Automatics (VNIIA), 127055 Moscow, Russia*
[4] *Faculty of Science and Technology and MESA+ Institute for Nanotechnology, University of Twente, 7500 AE Enschede, Netherlands*
[5] *Skobeltsyn Institute of Nuclear Physics, Lomonosov Moscow State University, 119991 Moscow, Russia*

submitted 9 Septemper 2023, accepted 24 November 2023, published 8 December 2023

**Terahertz time-domain spectroscopy is used to perform the first detailed studies of the electrodynamic properties of MoRe (60%/40%) films with thicknesses ranging from 10 to 100 nm. Films are prepared by magnetron sputtering technique on silicon substrates. The critical temperatures vary from 6.5 K (for 10 nm film) to 9.5 K (for 100 nm film). Spectra of complex permittivity, conductivity, refraction index, surface impedance and reflection coefficient for the films are acquired at frequencies 0.15–2.4 THz (wavenumbers 5–80 cm$^{-1}$) and in the temperature interval $T$ = 5–300 K. For all films, temperature dependencies of the superconducting energy gap, penetration depth, superconducting condensate plasma frequency, and normalised superfluid density are obtained on a quantitative level. It is shown that the reduction of film thickness leads to a strong decrease of the critical temperature and magnitude of the energy gap. The observed suppression of superconductivity is assigned to reduction of the superconducting order parameter due to the contribution to the free energy of the electronic energy states at the surface of superconductor. The MoRe films with the obtained characteristics can be used in designing advanced superconducting electronic devices.**

## Introduction

Molybdenum-rhenium superconducting alloys continue to attract the attention of researchers from a fundamental viewpoint because of their intriguing properties in the superconducting (SC) state as well as their significant potential for use in modern electronics. $Mo_{1-x}Re_x$ films exhibit superconductivity with a superconducting critical temperature $T_c$ reaching up to 15 K,[1–4] which is of the order of magnitude higher than $T_c$ = 0.9 K in Mo and $T_c$ = 1 K in Re.[5] The compounds are $s-$wave type-II superconductors, with the upper critical field of 8 T at 4 K.[6–8] There are indications of a two-band/two-gap superconductivity in the MoRe alloys[9,10] allowing to consider them as materials for the studies of multiband superconductivity. As an intriguing property, one can consider an electronic topological transition that is observed around the critical concentration $x_c$ = 0.11[11–13] making MoRe an ideal playground for study of time-reversal symmetry breaking in unconventional superconductors.[14]

Thin MoRe films exhibit excellent superconducting properties,[15] stable chemical, electrical and mechanical characteristics,[15–17] high radiation stability,[18] ability to make good electrical contact with carbon-based materials (graphene, carbon nanotubes),[19] stability for electron beam lithography.[20] All of these properties have revived a lively interest in MoRe alloys in the context of their use in developing elements for modern electronic systems. As a transparent for carriers interface to graphene and carbon nanotubes,[8,19] MoRe films are promising for the development of elements for quantum computation[21,22] and quantum memory.[23,24] Few nanometers thick MoRe films can be used for the fabrication of SQUID-on-tip devices with enhanced characteristics[20,25] and spin-qubit elements.[26,27]

The growing interest in thin MoRe films has emerged among communities working on developing sensitive single-photon detectors.[15,28] These detectors commonly use NbN thin films with the critical temperature $T_c$ close to 9 K (for a 4 nm-thick film).[28] With the doubled SC energy gap $2\Delta \approx 6$ meV (for 15 nm thick film),[29] high quantum efficiency NbN-based detectors operating in visible and middle infrared spectra regions can be realized.[28] To achieve even lower, terahertz (THz) working frequencies, superconductors with smaller gap values are necessary. Numerous compounds fit this requirement, such as MoSi ($2\Delta(0)$ = 2.28 meV), MoGe ($2\Delta(0)$ = 2.2 meV), WSi ($2\Delta(0)$ = 1.52 meV), and NbSi ($2\Delta(0)$ = 0.94 meV), as reported in Ref.[30] (here $\Delta(0)$ stands for the SC energy gap at zero temperature). However, their critical temperatures are rather low even for bulk samples. Thin MoRe films stand out because of their relatively high $T_c$ values, which is close to that for NbN films.

Thus, detailed studies of the electrodynamic properties of MoRe films in sub-terahertz and terahertz frequency domains are needed. In this frequency range the temperature evolution of the superconducting gap can be spectroscopically traced in detail and analyzed. In addition, operating frequencies of electronic communication systems of the next generation indeed belong to this range. Since such studies have not been reported so far, our goal was to perform the first systematic measurements and analyses of the electrodynamic characteristics of $Mo_{0.6}Re_{0.4}$ films with various thicknesses at frequen-

cies $f = 0.15 - 2.4\,\mathrm{THz}$ (wavenumbers $\nu = 1/\lambda_{\mathrm{cm}} = 5 - 80\,\mathrm{cm}^{-1}$, where $\lambda_{\mathrm{cm}}$ is radiation wavelength in cm) and in the temperature interval $T = 5 - 300\,\mathrm{K}$.

## Results and discussion

**Experimental procedure.** The $Mo_{0.6}Re_{0.4}$ films were prepared by magnetron sputtering on highly insulating and thus transparent for terahertz radiation silicon substrates of thickness ≈0.5 mm, as described in Ref. [20] Films thicknesses were 10, 15, 20, 30, 50, 70, and 100 nm. Terahertz characteristics of the films were determined using the commercial TeraView TPS Spectra 3000 time-domain spectrometer by measuring complex-valued (amplitude and phase) transmission coefficient spectra of the films on the substrates. Temperature-dependent THz spectra of the real parts of permittivity $\varepsilon'(\nu, T)$ and conductivity $\sigma'(\nu, T)$ of the MoRe films were calculated with the TeraCalc software. This employs numerical solution of the system of two essentially non-linear equations for the amplitude $Tr(\varepsilon', \sigma')$ and the phase $\varphi_{Tr}(\varepsilon', \sigma')$ of the complex transmission coefficient $Tr(\varepsilon', \sigma')\,\exp[i\varphi_{Tr}(\varepsilon', \sigma')]$ of a two-layered system (a film on a substrate), see Eqs. (1)–(5) in Supporting Information. Other quantities, such as the real and imaginary parts of the complex refractive index $n^* = n + ik$, and the surface impedance $Z_s = R_s + iX_s$, were also calculated using standard expressions (see, *e. g.*, textbook[31]). THz parameters of the Si substrates were determined beforehand. Measurements were performed in a quasi-optical configuration of the measurement scheme of the spectrometer, with a homemade helium-flow cryostat equipped with Mylar windows.

**Normal state.** Figure 1a shows room-temperature spectra of transmission coefficient $Tr$ of the bare silicon substrate and of substrates with $Mo_{0.6}Re_{0.4}$ films of thickness 10, 20, 50, and 100 nm. The periodic oscillations in the spectra arise from the interference of the electromagnetic waves inside the plane-parallel transparent substrate, which can be considered as a Fabry-Pérot resonator. The interval $\Delta\nu$ between oscillations is mainly determined by the substrate refraction index $n$ and thickness $d$: $\Delta\nu = (2nd)^{-1}$, while the amplitudes of the peaks are determined by the transparency of the films. For the bare substrate, the transmission of the interferometric peaks reaches nearly unity, while the transmission of the peaks for the samples with MoRe films is significantly lower (at about two orders of magnitude for the 100 nm thick film). There is a phase shift at about $\pi$ between the maxima observed for the bare substrate and the substrates covered with MoRe films. This is a consequence of impedance matching of the silicon-air interface by conducting $Mo_{0.6}Re_{0.4}$ film with a thickness smaller than the skin depth. The phenomenon was considered in detail in Refs.[32,33]

Spectra of transmission coefficient of all samples, as well as frequency dependences of conductivity and permittivity of all films did not reveal any significant changes during cooling from 300 K down to the critical temperature $T_c$, in accordance with the literature data.[34] At all

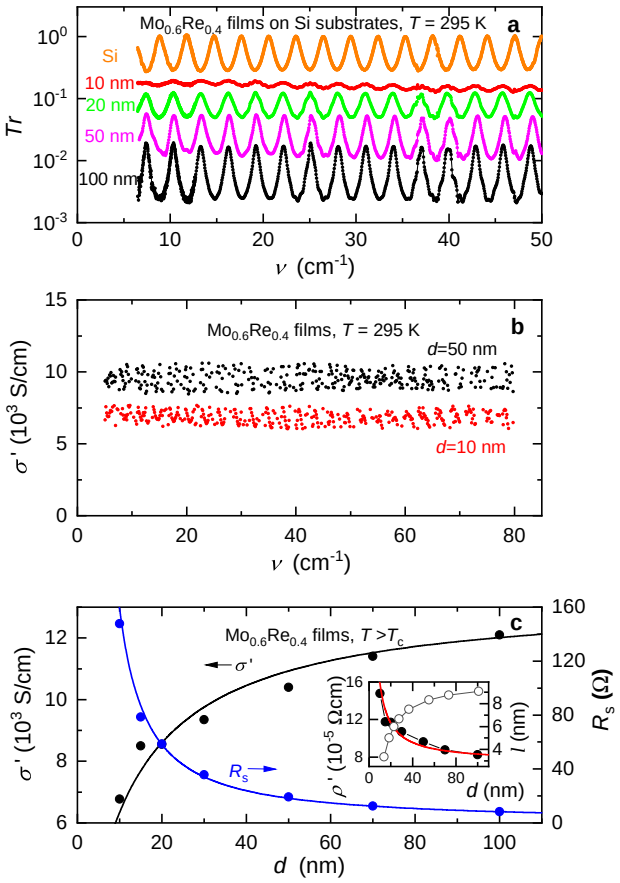


**Figure 1.** **a** – Room-temperature spectra of the transmission coefficient of $Mo_{0.6}Re_{0.4}$ films of various thicknesses deposited on silicon substrates. Periodic oscillations are due to the Fabry-Pérot effect – *i. e.* interference of electromagnetic waves inside plane-parallel substrate. **b** – Room-temperature dispersionless conductivity spectra of $Mo_{0.6}Re_{0.4}$ films of thickness $d = 50$ nm and $d = 10$ nm. **c** – Thickness dependence of AC conductivity $\sigma'$ (left axis) and surface resistance $R_s = (\sigma' d)^{-1}$ (right axis) in the normal state ($T > T_c$). Inset shows thickness dependence of AC resistivity $\rho' = 1/\sigma'$ and mean-free path $l$, determined from fit of $\rho'(d)$ with Eq. (1), for charge carriers in the films. Lines show least-square fits based on expression (1) from Ref.[35]

temperatures in the normal state (at $T > T_c$) the conductivity spectra of all films were dispersionless, indicating the metal-type response in the low-frequency limit ($\nu \ll \gamma$, where $\gamma$ is the scattering rate of carriers) of the Drude conductivity model.[36,37] This is demonstrated in figure 1b, where the conductivity spectra of two films, 10 nm and 50 nm thick, are shown as examples. Figure 1c shows the dependence of the normal-state AC conductivity $\sigma'$, AC resistivity $\rho' = 1/\sigma'$, and surface impedance $(\sigma' d)^{-1}$ on the thickness $d$ of the MoRe films. It is seen that the dependences are well described by the following expression obtained for granular films accounting additional scattering effects at film surface and grain boundaries[38]

$$\rho(d) = \rho_0 \left(1 + A\,\frac{l_0}{d}\right). \qquad (1)$$

Here, $\rho_0$ and $l_0$ are the bulk resistivity and the bulk mean free path of the charge carriers, respectively, and $A$ is a constant of the order of unity. Fitting the $\rho(d)$ depen-

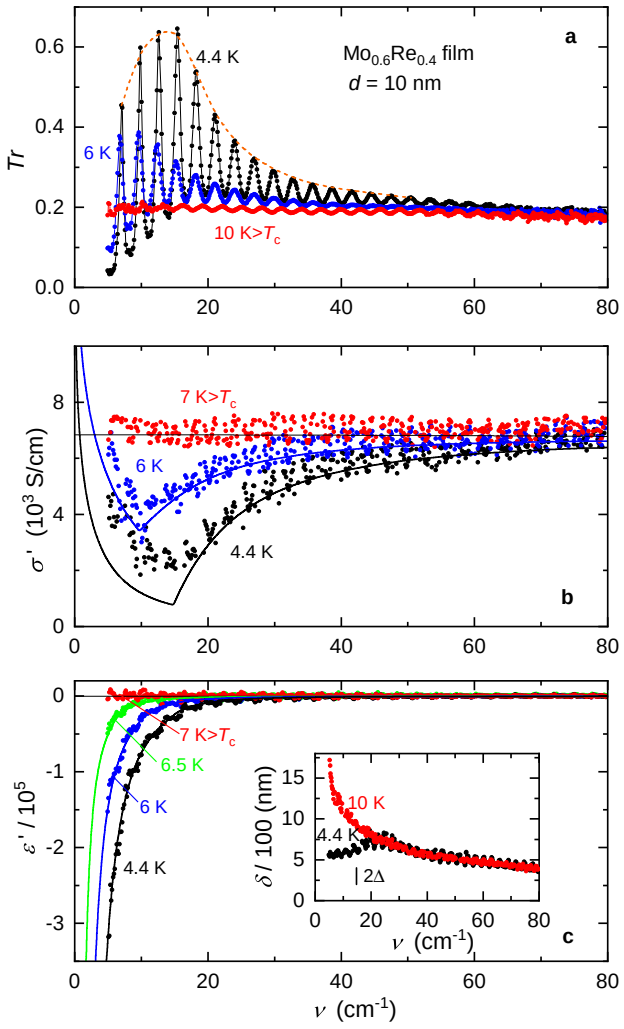


**Figure 2.** **a**, **b**, **c** – Frequency dependence of the transmission coefficient (**a**), the real part of AC conductivity (**b**), and the real part of dielectric permittivity (**c**) for 10 nm-thick $Mo_{0.6}Re_{0.4}$ film on silicon substrate, measured at different temperatures above and below $T_c$. Oscillations in the spectra in panel **a** are due to the interference of radiation within the plane-parallel Si substrate. Red dashed envelope line shows that the oscillations at $T = 4.4$ K display broad maximum around the value $2\Delta/hc$. Inset in panel **c** represents radiation penetration depth[39] $\delta = (2\pi k\nu)^{-1}$ above and below $T_c$ (here $k$ is the extinction coefficient); vertical bar marks SC energy gap at 4.4 K. Solid lines in panels **b** and **c** are the least-square fits with BCS expressions.[40]

dence by Eq. (1) allows to determine $l_0 = 10$ nm and $\rho_0 = 75\,\mu\Omega\cdot$cm. The value $l_0 = 10$ nm is more than two times larger than $l = 4.2$ nm obtained for MoRe alloy.[14] Taking the Fermi velocity $v_F = 2.34 \cdot 10^7$ cm/s,[14] we estimate the scattering rate of charge carriers $\gamma = v_F/(2\pi c l_0) \approx 120\,\text{cm}^{-1}$ (c is the speed of light). This value lies above our working frequency interval, thus confirming that the normal-state response of the films corresponds to the low-frequency limit of the Drude conductivity model.

**Superconducting state.** Spectra of transmission coefficient, conductivity and permittivity of all studied films undergo strong changes when these films enter the SC state. This is demonstrated in figure 2 by the spectra obtained for 10 nm-thick MoRe film on silicon substrate (see also the spectra for 50 nm-thick MoRe film on silicon substrate in figure S1 in Supporting Information). These changes are typical for SC films as it was first demonstrated by Tinkham and coworkers[41–44] and reproduced later by other researchers in numerous experiments on conventional and high-$T_c$ superconductors. As described below, by analyzing the spectra of the real parts of conductivity ($\sigma'$) and permittivity ($\varepsilon'$) through model fitting, we enable accurate determination of the critical temperature $T_c$ (with an accuracy ±0.2 K) and the energy gap $\Delta$ (with an accuracy ±0.14 meV), as well as other characteristics of the SC state for MoRe films. At the lowest achievable temperature $T = 4.4$ K, the envelope for the interferometric peaks in the transmission spectrum (dashed red line in figure 2a) displays broad maximum around the value $2\Delta/hc$ (where $h$ is Planck's constant), corresponding to the SC gap. The THz conductivity that characterizes absorption of radiation becomes suppressed at below $50 - 60\,\text{cm}^{-1}$, showing a kink around $2\Delta/hc$ (figure 2b). Also, the dielectric permittivity strongly decreases below $20\,\text{cm}^{-1}$ (see Ref.[45]) according to the relationship $\varepsilon' = -(\nu_{pl}^{SC}/\nu)^2$ representing dielectric response of SC condensate, where $\nu_{pl}^{SC} = (2\pi c)^{-1}\sqrt{4\pi n_e e^2/m^*}$ is the plasma frequency of SC condensate, $n_e$ is the density of electrons in SC condensate, $e$ is the electron charge, and $m^*$ is the electron effective mass. The dielectric permittivity reaches large negative values that characterise the inductive response of Cooper-pairs condensate under the zero-frequency delta function in the conductivity spectrum. The superconducting transition also leads to strong changes in other electrodynamic quantities. Figure 3 shows the temperature evolution of the spectra of real and imaginary parts of the complex refraction coefficient $n^* = n + ik$ of the 10 nm-thick film (similar data for 50 nm-thick film is shown in figure S2). In the normal state, $n \approx k \sim (\sigma'/\nu)^{0.5}$, as expected for a good conductor.[36,37] Below $T_c$, the extinction coefficient $k$ strongly increases and refraction index $n$ decreases, leading to a strong enhancement in the bulk reflection coefficient $R$ below $2\Delta/hc$ (inset in figure 3b).[†] Similar spectra for the 50 nm-thick film are presented in figure S2. One can see in figures 2b and 3a that in the SC state at low wavenumbers, $\nu < 2\Delta/hc$, there is significant scattering in the experimental data for the conductivity $\sigma'$ and the refraction index $n$; it is especially pronounced for the 50 nm-thick film (figures S1 and S2). The reason is that the transmission spectra measured in the SC state are mainly determined by the large negative permittivity $\varepsilon'$ and the large positive extinction coefficient $k$. As a result, both quantities $\varepsilon'$ and $k$ are determined much more precisely compared to $\sigma'$ and $n$.[32,33,46]

To add more to the THz electrodynamic properties of

[†]Note that an ideal $s-$wave superconductor at $T = 0$ and $\nu < 2\Delta/hc$ would have zero AC conductivity $\sigma'$ and large negative permittivity $\varepsilon'$ values leading to $n = 0$ and $k \gg 1$. This case would correspond to an ideal reflector with a bulk reflection coefficient[31] $R_{bulk} = [(n-1)^2 + k^2]/[(n+1)^2 + k^2] = 1$.

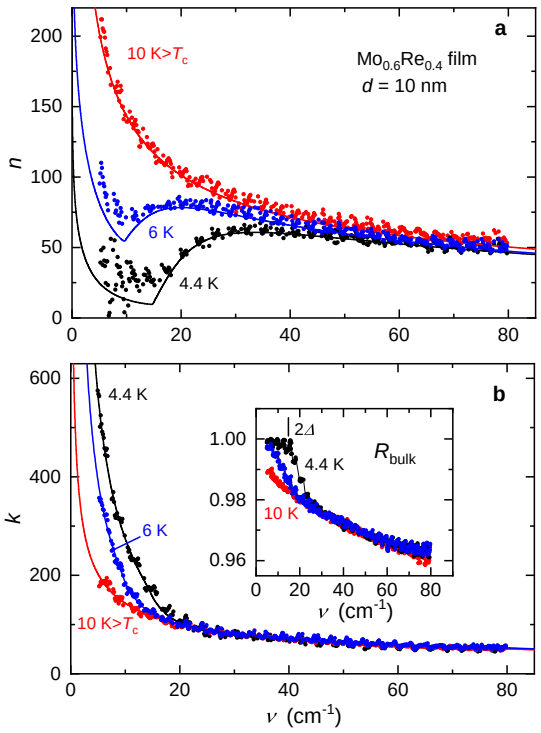


**Figure 3.** **a**, **b** – Frequency dependence of the refraction coefficient (**a**) and the extinction coefficient (**b**) for 10 nm-thick $Mo_{0.6}Re_{0.4}$ film on silicon substrate measured at temperatures above and below $T_c$. Solid lines in panel **b** for $T = 4.4$ K and $T = 6$ K are the least-square fits with BCS expressions;[40] lines corresponding to normal-state spectra at $T = 10$ K are plotted according to the low-frequency limit ($\nu \ll \gamma$) of the Drude conductivity model:[36,37] $n \approx k \approx (\sigma'/\nu)^{0.5}$. Inset in panel **b** shows spectra of the bulk reflection coefficient calculated according to the expression $R_{bulk} = [(n-1)^2+k^2]/[(n+1)^2+k^2]$; vertical bar marks SC energy gap at 4.4 K.

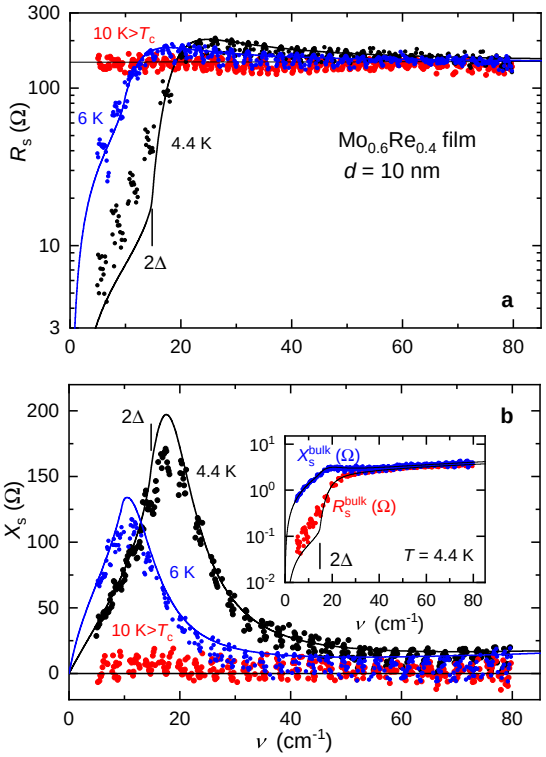


**Figure 4.** **a**, **b** – Frequency dependence of the real $R_s$ (**a**) and the imaginary $X_s$ (**b**) parts of the surface impedance $Z_s = R_s + iX_s = (\sigma^* d)^{-1} = \sigma'/[d(\sigma'^2+\sigma''^2)] + i\sigma''/[d(\sigma'^2+\sigma''^2)]$ of 10 nm-thick $Mo_{0.6}Re_{0.4}$ film on silicon substrate measured at temperatures above and below $T_c$; $\sigma^* = \sigma' + i\sigma''$ is the complex conductivity. Solid lines are the least-square fits with BCS expressions.[40] Inset in panel **b** shows $R_s$ and $X_s$ spectra of bulk material calculated using the formulas $R_s = Z_0 n/(n^2+k^2)$, and $X_s = Z_0 k/(n^2+k^2)$, where $Z_0 = 376.7\,\Omega$. In normal state $|R_s| \approx |X_s|$, as expected in the low-frequency limit ($\nu \ll \gamma$) of the Drude conductivity model;[36] at $T < T_c$ both quantities strongly decrease.[48] Vertical bar marks SC energy gap at 4.4 K.

the studied $Mo_{0.6}Re_{0.4}$ films, we present in figure 4 the spectra of the real $R_s$ and imaginary $X_s$ parts of surface impedance $Z_s = R_s + iX_s$. For a thin film, it reads $Z_s = (\sigma^* d)^{-1} = \sigma'[d(\sigma'^2+\sigma''^2)]^{-1} + i\sigma''[d(\sigma'^2+\sigma''^2)]^{-1}$, where $\sigma^* = \sigma' + i\sigma''$ is the complex-valued conductivity of the film material. At $T > T_c$ we observe dispersionless dependences $R_s$ and $X_s \approx 0$ on the wavenumber, as expected for a good conductor.[37,47] In the SC state, the real impedance $R_s$ (related to absorption) is strongly suppressed, while the frequency dependence of $X_s$ has a broad maximum around the doubled gap frequency. These findings are typical fingerprints of a superconducting response.[48]

Although MoRe compounds are considered as two-band superconductors,[9,10] we do not observe any corresponding feature in the measured THz spectra (figures 2–4, as well as figures S1 and S2). The reason might be that the contribution to the electrodynamic response of one of the bands considerably exceeds the contribution of the other band. Thus, in order to model the experimental spectra, we used the BCS expressions derived for a single-band superconductor.[40] The fitting results shown by the solid lines in figures 2–4, S1–S2 describe the experimental spectra quite well. From figure 2b we see that the measured conductivity values are slightly above the BCS results, indicating extra below-gap absorption that may be due to bulk and/or surface defects. The performed fitting of the spectra allows us to determine temperature dependences of characteristics of the SC condensate – namely, the plasma frequency $\nu_{pl}^{SC}$, the London penetration depth $\lambda_L = 1/(2\pi\nu_{pl}^{SC})$, the normalised superfluid density $1/\lambda_L^2$ and the energy gap (figure 5). The temperature dependences of $\nu_{pl}^{SC}$, $\lambda_L$ and $1/\lambda_L^2$ are in agreement with the expressions of two-fluid superconductivity model:[47]

$$\nu_{pl}^{SC}(T) = \nu_{pl}^{SC}(0)\sqrt{1-(T/T_c)^4}, \tag{2}$$

$$\lambda_L(T) = \frac{\lambda_L(0)}{\sqrt{1-(T/T_c)^4}}, \tag{3}$$

The temperature dependences of the gap energy values for the MoRe films of different thicknesses are well described by the BCS-like empirical expression[49]

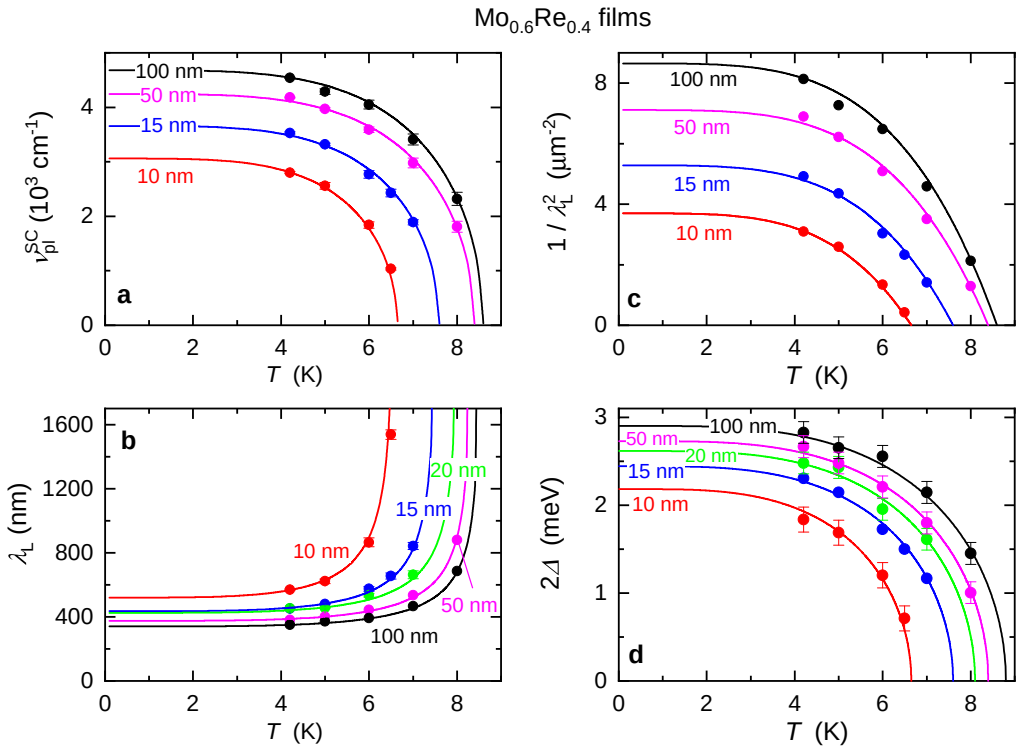


**Figure 5.** **a**, **b**, **c** – Temperature dependences of the plasma frequency of superconducting condensate $\nu_{pl}^{SC}$ (**a**), the London penetration depth $\lambda_L$ (**b**), and the normalized superfluid density $1/\lambda_L^2$ (**c**) for the MoRe films of various thicknesses. Lines show least-square fits using expressions of the phenomenological Gorter-Cazimir two-fluid model of superconductivity,[47] corresponding expressions (2) and (3) are given in the text. **d** – Temperature dependences of the superconducting energy gap values for $Mo_{0.6}Re_{0.4}$ films of different thicknesses. Solid lines show the least-square fits with the empirical expression[49] (4).

$$2\Delta(T) \simeq 2\Delta(0)\ \tanh\left\{1.82\left[1.081\left(\frac{T_c}{T}-1\right)\right]^{0.51}\right\}. \quad (4)$$

In the above expressions (2)–(4) $\nu_{pl}^{SC}(0)$, $\lambda_L(0)$, and $2\Delta(0)$ represent zero-temperature values of the corresponding quantities. The doubled SC gap values obtained for all films are below 3 meV, so that the corresponding gap frequencies $2\Delta(0)/hc < 24\,\mathrm{cm}^{-1}$ are smaller than the estimated scattering rate $\gamma \approx 120\ \mathrm{cm}^{-1}$. This means that we deal with the dirty-limit superconductivity for all tested MoRe films.

Earlier, it was shown[9] that the superfluid density in $Mo_{0.6}Re_{0.4}$ polycrystalline samples cannot be explained within the framework of a single-band approach, since they show clear deviation from single-band behavior at low temperatures 2-6 K. Those data were described considering a two-band approach with the energy gaps $2\Delta_1 = 3.9$ meV and $2\Delta_2 = 1$ meV. The gap value $2\Delta(0) = 2.9$ meV obtained in our experiment for the thickest (100 nm) film falls between $2\Delta_1$ and $2\Delta_2$.

**Thickness dependence of THz characteristics of $Mo_{0.6}Re_{0.4}$ films in superconducting state.** Figure 6 presents the dependences of the penetration depth $\lambda_L(0)$, the critical temperature $T_c$ and the SC gap energy $2\Delta(0)$ on the thickness $d$ of the MoRe films. The reduction of the film thickness leads to an increase of the penetration depth and the decrease in both the critical temperature and zero-temperature energy gap. The ratio $2\Delta(0)/k_BT_c = 3.8 \pm 0.2$ is slightly higher than the standard BCS value 3.52 for weak-coupling regime, and this indicates moderately strong electron-phonon coupling in the MoRe films ($k_B$ is the Boltzmann constant). By fitting the experimental dependence of $\lambda_L(0)$ on $d$ using the expression[50]

$$\lambda_L(d) = 0.62\,\lambda_0\sqrt{\frac{\xi_0}{l(d)}}, \quad (5)$$

which is valid in the dirty limit, we are able to estimate the bulk BCS coherence length $\xi_0 = 26$ nm; $\lambda_0$ corresponds to the bulk penetration depth. The result of the fitting is shown in figure 6a by solid line. Taking $2\Delta(0) = 3$ meV as typical energy gap for bulk material (according to figure 6c) and the Fermi velocity[14] $v_F = 2.34 \cdot 10^7$ cm/s and using well-known expression[50] $\xi_0 = \hbar v_F/(\pi\Delta)$, we get the value of the BCS coherence length $\xi_0 \approx 33$ nm that is close to the above estimate $\xi_0 = 26$ nm. It makes possible to estimate the Ginsburg-Landau parameter $\kappa = \lambda_L/\xi \sim 10$, indicating type-II superconductivity in MoRe films. Using the dirty-limit expression[50]

$$\xi(d) = 0.855\sqrt{\xi_0 l(d)}, \quad (6)$$

we can evaluate the dependence of the coherence length

$\xi$ on film thickness. The result is shown in the inset of figure 6a together with the thickness dependence of the mean free path $l$. For all films, we have $\xi(d) > l(d)$, what again confirms the dirty-limit SC. Smallness of the coherence length $\xi$ and the mean free path $\ell$ with respect to both the penetration depth in normal state $\delta = (2\pi k\nu)^{-1}$ and in SC state $\lambda_L$ (see insets in figures 2c, S1c, and 5b) means that the local approach holds in the normal and SC states of the studied $Mo_{0.6}Re_{0.4}$ films.

Let us consider the suppression of superconductivity in thin films that is accompanied by a reduction of both the critical temperature and the energy gap. Since $Mo_{0.6}Re_{0.4}$ films are binary alloy, such suppression could be due to disorder. Maekawa and Fukuyama[51] were the first to analyze the suppression caused by Cooper pairs localization in disordered thin films leading to an enhanced Coulomb repulsion and suppressed electronic density of states. They obtained the following expression

$$\ln\left(\frac{T_c}{T_c^{bulk}}\right) = -\frac{1}{2}\frac{(g_1 - 3g')N(0)e^2R_\square}{2\pi^2\hbar}\left[\ln\left(5.5\frac{\xi_0}{l}\frac{T_c^{bulk}}{T_c}\right)\right]^2 - \frac{1}{3}\frac{(g_1 + g')N(0)e^2R_\square}{2\pi^2\hbar}\left[\ln\left(5.5\frac{\xi_0}{l}\frac{T_c^{bulk}}{T_c}\right)\right]^3, \quad (7)$$

where $g' < 0$ stands for the attractive interaction responsible for Cooper pair formation, $g_1 > 0$ characterizes Coulomb repulsion, $N(0)$ is the electronic density of states at the Fermi level per spin, $R_\square$ is the sheet resistance, and $T_c^{bulk}$ is the critical temperature of bulk sample. The expression (7) with the parameters $g' = -0.2$ and $g_1 = 7$ describes the experimental $T_c(d)$ data quite well (dashed line in figure 6b), but the value $g_1 = 7$ seems to be too large as compared with $g_1 \sim 1$, considered in Maekawa and Fukuyama's paper.

Alternatively, we can use the theory of Finkel'shtein[52] based on the renormalization group approach and leading to the following expression

$$\frac{T_c}{T_c^{bulk}} = e^{-1/\gamma}\left[\frac{1 + \sqrt{t/2}/(\gamma - t/4)}{1 - \sqrt{t/2}/(\gamma - t/4)}\right]^{1/\sqrt{2t}}, \quad (8)$$

where $t = e^2R_\square/(2\pi^2\hbar)$, $\gamma = 1/\log(T_c^{bulk}\tau)$, and $\tau$ is the transit time. Taking the Fermi velocity $v_F = 2.34 \times 10^7$ cm/s[14] and thickness-dependent mean free path (see inset of figure 6a), we conclude that the expression (8) cannot reproduce our experimental data (see red line in the inset of figure 6b), since we should consider unreasonably short bulk mean free path, $l_0 = 0.56\,\AA$ (see blue line in the inset of figure 6b).

Following the paper of Simonin[53] we consider a surface contribution[‡] to the Ginzburg-Landau free energy functional that leads to decrease in the density of states near the surface. This effect becomes significant in thin films where the surface-to-volume ratio is dominant. The theory of Simonin predicts the following dependence

$$T_c(d) = T_c^{bulk}\left(1 - \frac{d_c}{d}\right), \quad (9)$$

where $d_c = 2a/N(0)V$ is the critical thickness, corresponding to $T_c = 0$, $a$ is the Thomas-Fermi screening length that is of the order of lattice parameter, $V$ is the interaction potential, and $N(0)V$ is the bulk interaction potential. The expression (9) describes well the experimental data with the ratio $2a/N(0)V = 1.2$ nm (solid line in figure 6b). Taking $a \approx 0.3$ nm for $Mo_{0.6}Re_{0.4}$, we

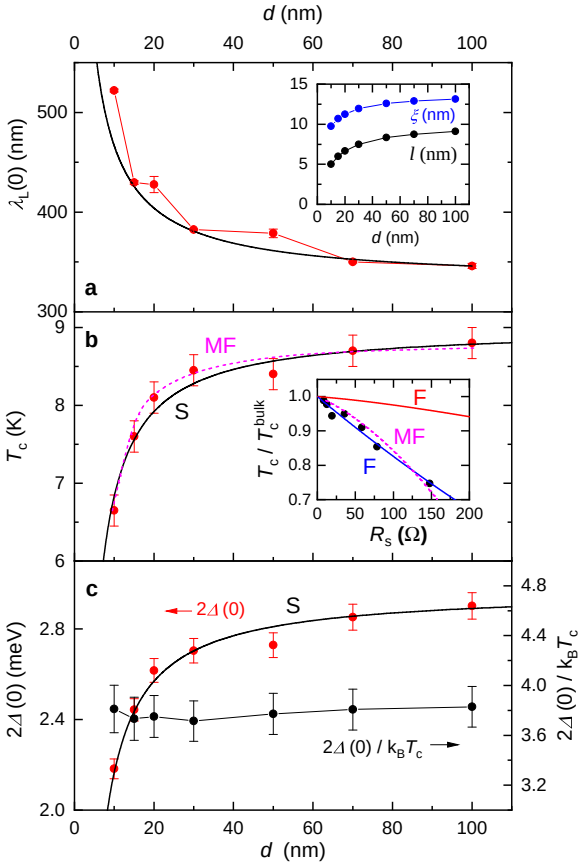


**Figure 6.** **a**, **b**, **c** – Thickness dependence of the zero-temperature London penetration depth $\lambda_L(0)$ (**a**), the critical temperature (**b**), the superconducting energy gap $2\Delta(0)$ and the ratio $2\Delta(0)/k_BT_c$ (**c**) for $Mo_{0.6}Re_{0.4}$ films. Solid line in panel **a** is the least-square fit according to Eq. (5). In panel **b** the dashed line (labelled MF) is a result of calculation according to the expression (7) taken from Maekawa and Fukuyama's paper,[51] and solid line (labelled S) corresponds to the least-square fit with the expression (9) taken from Simonin's paper.[53] In panel **c** the solid line (S) shows a fit with $2\Delta(d) \sim (1 - \text{const}/d)$, see Eq. (9). Inset in panel **a**: thickness-dependent coherence length and electron mean free path. Inset in panel **b**: dots – the dependence of the critical temperature of $Mo_{0.6}Re_{0.4}$ films on their surface resistance; dashed line (MF) – least-square fit with expression (7); blue line (labelled F) – fit according to the expression (8) taken from Finkel'shtein's paper[52] ($v_F = 2.34 \cdot 10^7$ cm/s and $l_0 = 0.56\,\AA$); red line (F) – calculation using the expression (8) with the same parameters as before, but with the thickness-dependent mean free path, see inset in panel **a**.

[‡]The author adds the term proportional to an integral $\int_S \psi^2 ds$ over the surface of a superconductor into the free-energy functional, where $\psi$ is the normalized order parameter. This leads to the modification of the boundary conditions and results in the suppression of $T_c$.

obtain a quite reasonable value for the interaction potential $N(0)V \approx 0.5$. This allows us to conclude that the reduction of the order parameter near the surfaces of SC films can be considered as a more appropriate mechanism of suppression of superconductivity in the studied films. We note that similar results have been obtained for pure molybdenum films.[54]

According to figure 6c, the ratio $2\Delta/k_BT_c = 3.8 \pm 0.2$ seems to be thickness-independent, suggesting that the critical temperature depends on the film thickness in the same way as the energy gap. This is demonstrated by a fit of the experimental dependence $2\Delta(d)$ with an expression $2\Delta(d) \sim (1 - \text{const}/d)$ that is similar to Eq. (9). We thus suggest that the suppression of both the critical temperature and the SC energy gap are governed by the same mechanism – the alteration of the boundary conditions caused by the surface term introduced in the GL functional, resulting in change of the interaction potential $N(0)V$.

## Conclusion

The first systematic studies of terahertz electrodynamic properties of $Mo_{0.6}Re_{0.4}$ films of thicknesses ranging from 10 to 100 nm and corresponding critical temperatures from 6.5 to 9.5 K are performed at frequencies $0.15 - 2.4$ THz and in the temperature interval $T = 5 - 300$ K. The spectra of conductivity and permittivity are described within the BCS single-band approach. The obtained ratio $2\Delta(0)/k_BT_c = 3.8 \pm 0.2$ slightly exceeds the BCS value 3.52, demonstrating moderately strong electron-phonon coupling. The temperature dependencies of the superconducting energy gap, the penetration depth, the superconducting condensate plasma frequency and the normalized superfluid density are reproduced within the two-fluid superconductivity model. A strong decrease in the critical temperature and the energy gap in thin MoRe films is associated with the suppression of the mean superconducting order parameter due to a decrease in the local electronic density of states in MoRe films near their surfaces. Although our thinnest films have slightly smaller values of the critical temperature than those obtained earlier,[28] the values $T_c(d)$ are still higher than the critical temperatures of the alloys[30] MoSi, MoGe, WSi, NbSi, mentioned in the Introduction section. This makes MoRe alloy a perspective material for the design of elements and devices of advanced electronics and optoelectronics, for example, single-photon detectors, high-Q resonators for frequency locking systems (see figure S3), etc.

## Acknowledgements

This work was supported by RSF 23-72-30004 (terahertz experiments and data analysis). Magnetron sputtering fabrication supported by the Ministry of Science and Higher Education of the Russian Federation (No. FSMG-2022-0014).

## Supporting information and data availability

The Supporting Information is available free of charge at https://jmsn.colab.ws/publications/01-01002/supporting-file.

The data that support the findings of this study are available from the corresponding authors upon request.

## Contact information

Corresponding author: Boris M. Nekrasov, orcid.org/0000-0003-3324-2893, e-mail nekrasov.bm@phystech.edu.

Corresponding author: Vasily S. Stolyarov, orcid.org/0000-0002-5317-0818, e-mail stolyarov.vs@phystech.edu.

## Author contribution

Elena S. Zhukova, Alexander V. Melentev and Lenar S. Kadyrov carried out the THz experiments, spectra processing and data analysis. Boris M. Nekrasov, Anton S. Shaimardanov, Andrey G. Shishkin, Aleksander A. Golubov, Mikhail Yu. Kupriyanov performed data analysis, Boris P. Gorshunov and Vasily S. Stolyarov conceived and supervised the work. All authors contributed to the manuscript.

## Competing Interests

The authors declare no competing financial or non-financial interests.

## References

[1] Testardi L. R., Hauser J. J., Read M. H. *Enhanced superconducting $T_c$ and structural transformation in Mo-Re alloys.*. Solid State Commun., vol. **9**, 1829-1831 (1971).

[2] Gavaler J. R., Janocko M. A., Jones C. K. *A-15 structure Mo-Re superconductor*. Appl. Phys. Lett., vol. **21**, 179-180 (1972).

[3] Postnikov V. S., Postnikov V. V., Zheleznyi V. S. *Superconductivity in Mo-Re system alloy films produced by electron beam evaporation in high vacuum*. Physica Status Solidi (a), vol. 39, K21-K23 (1977).

[4] Gavaler J. R., Janocko M. A., Jones C. K. *Superconductivity and Metastability in Alloys of the Mo-Re System*. In: Timmerhaus, K. D., O'Sullivan, W. J., Hammel, E. F. (eds) Low Temperature Physics–LT 13. Springer, Boston, MA (USA), 558-562 (1974).

[5] Vonsovsky S. V., Izyumov Y. A., Kurmaev E. Z. *Superconductivity of transition metals: their alloys and compounds*. Springer Series in Solid-State Sciences, vol. **27** (1982).

[6] Faley M. I., Reith P., Satrya C. D., Stolyarov V. S., Folkers B., Golubov A. A., Hilgenkamp H., Dunin-Borkowski R. E. *MoRe/YBCO Josephson junctions and $\pi$-loops*. Superconductor Sci. Technol., vol. **33**, 044005 (2020).

[7] Amet F., Ke C. T., Borzenets I. V., Wang J., Watanabe K., Taniguchi T., Deacon R. S., Yamamoto M., Bomze Y., Tarucha S., Finkelstein G. *Supercurrent in the quantum Hall regime*. Science, vol. **352**, 966-969 (2016).

[8] Calado V. E., Goswami S., Nanda G., Diez M., Akhmerov A. R., Watanabe K., Taniguchi T., Klapwijk T. M., Vandersypen L. M. K. *Ballistic Josephson junctions in edge-contacted graphene*. Nature Nanotechnology, vol. **10**, 761-764 (2015).

[9] Sundar, S., Sharath Chandra, L. S., Chattopadhyay, M. K., Roy, S. B. *Evidence of multiband superconductivity in the $\beta-$phase $Mo_{1-x}Re_x$ alloys*. J. Phys.: Condens. Matt., vol. **27**, 045701 (2015).

[10] Tarenkov V., Shapovalov A., Boliasova O., Belogolovskii M., Kordyuk A. *Two-band superconductivity in a Mo-Re alloy with an equal concentration of the components*. Low Temp. Phys., vol. **47**, 101-105 (2021).

[11] Gornostyrev Y. N., Katsnelson M. I., Peschanskikh G. V., Trefilov A. V. *On the Nature of the Rhenium Effect. Peculiarities of the Band Structure and Elastic Moduli of W-and Mo-Based Alloys*. Physica Status Solidi (b), vol. **164**, 185-193 (1991).

[12] Okada M., Rotenberg E., Kevan S. D., Schäfer J., Ujfalussy B., Stocks G. M., Genatempo B., Bruno E., Plummer E. W. *Evolution of the electronic structure in $Mo_{1-x}Re_x$ alloys*. New J. Phys., vol. **15**, 093010 (2013).

[13] Tarenkov V., Shapovalov A., Zhitlukhina E., Belogolovskii M., Seidel P. *Mo-Re alloy: A new benchmark two-band superconductor*. Low Temp. Phys., vol. **49**, 103-107 (2023).

[14] Shang T., Baines C., Chang L., Gawryluk D. J., Pomjakushina E., Shi M., Medarde M., Shiroka T. *$Re_{1-x}Mo_x$ as an ideal test case of time-reversal symmetry breaking in unconventional superconductors*. npj Quantum Materials, vol. **5**, 76 (2020).

[15] Seleznev V. A., Tarkhov M. A., Voronov B. M., Milostnaya I. I., Lyakhno V. Y., Garbuz A. S., Mikhailov M. Y., Zhigalina O. M., Gol'tsman G. N. *Deposition and characterization of few-nanometers-thick superconducting Mo-Re films*. Supercond. Sci. Technol., vol. **21**, 115006 (2008).

[16] Sundar S., Sharath Chandra L. S., Sharma V. K., Chattopadhyay M. K., Roy S. B. *Electrical transport and magnetic properties of superconducting $Mo_{52}Re_{48}$ alloy*. AIP Conf. Proc., vol. **1512**, 1092-1093 (2013).

[17] Mohsin A., David C. H., Saverio R. 1 *Molybdenum-rhenium superconducting suspended nanostructures*. Appl. Phys. Lett., vol. **104**, 233102 (2014).

[18] Andreone A., Baldini A., Borchi E., Del Carmine P., Di Chiara A., Mandò P. A., Persico V. *Radiation hardness of $Mo_{60}Re_{40}$ superconducting thin films*. Nucl. Phys. B – Proc. Suppl., vol. **44**, 688-692 (1995).

[19] Schneider B. H., Etaki S., van der Zant H. S., Steele G. A. *Coupling carbon nanotube mechanics to a superconducting circuit*. Sci. Rep., vol. **2**, 599 (2012).

[20] Shishkin A. G., Skryabina O. V., Gurtovoi V. L., Dizhur S. E., Faley M. I., Golubov A. A., Stolyarov V. S. *Planar MoRe-based direct current nanoSQUID*. Supercond. Sci. Technol., vol. **33**, 065005 (2020).

[21] Schmidt F. E., Jenkins M. D., Watanabe K., Taniguchi T., Steele G. A. *A ballistic graphene superconducting microwave circuit*. Nature Commun., vol. **9**, 4069 (2018).

[22] Yu C. G., Kim B., Doh Y.-J. *Fabrication and characterization of magnetic-field-resilient MoRe superconducting coplanar waveguide resonators*. Curr. Appl. Phys., vol. **47**, 24–29 (2023).

[23] Ranjan V., de Lange G., Schutjens R., Debelhoir T., Groen J. P., Szombati D., Thoen D. J., Klapwijk T. M., Hanson R., DiCarlo L. *Probing dynamics of an electron-spin ensemble via a superconducting resonator*. Curr. Appl. Phys., vol. **47**, 24-29 (2023).

[24] Amsüss R., Koller C., Nöbauer T., Putz S., Rotter S., Sandner K., Schneider S., Schramböck M., Steinhauser G., Ritsch H., Schmiedmayer J., Majer J. *Cavity QED with Magnetically Coupled Collective Spin States*. Phys. Rev. Lett., vol. **107**, 060502 (2011).

[25] Wang J. I., Rodan-Legrain D., Bretheau L., Campbell D. L., Kannan B., Kim D., Kjaergaard M., Krantz P., Samach G. O., Yan F., Yoder J. L., Watanabe K., Taniguchi T., Orlando T. P., Gustavsson S., Jarillo-Herrero P., Oliver W. D. *Coherent control of a hybrid superconducting circuit made with graphene-based van der Waals heterostructures*. Nature Nanotechnology, vol. **14**, 120-125 (2019).

[26] Borjans F., Croot X. G., Mi X., Gullans M. J., Petta J. R. *Resonant microwave-mediated interactions between distant electron spins*., Nature, vol. **577**, 195-198 (2020).

[27] Banszerus L., Hecker K., Möller S., Icking E., Watanabe K., Taniguchi T., Volk C., Stampfer C. *Spin relaxation in a single-electron graphene quantum dot*. Nature Commun., vol. **13**, 3637 (2022).

[28] Milostnaya I., Korneev A., Tarkhov M., Divochiy A., Minaeva O., Seleznev V., Kaurova N., Voronov B., Okunev O., Chulkova G., Smirnov K., Gol'tsman G. *Superconducting single photon nanowire detectors development for IR and THz applications*. J. Low Temp. Phys., vol. **151**, 591-596 (2008).

[29] Beck M., Klammer M., Lang S., Leiderer P., Kabanov V. V., Gol'tsman G. N., Demsar J. *Energy-gap dynamics of superconducting NbN thin films studied by time-resolved terahertz spectroscopy*. Phys. Rev. Lett., vol. **107**, 177007 (2011).

[30] Banerjee A., Baker L. J., Doye A., Nord M., Heath R. M., Erotokritou K., Bosworth D., Barber Z. H., MacLaren I., Hadfield R. H. *Characterisation of amorphous molybdenum silicide (MoSi) superconducting thin films and nanowires*. Supercond. Sci. Technol., vol. **30**, 084010 (2017).

[31] Born M., Wolf E., Bhatia A. B. *Principles of Optics: Electromagnetic Theory of Propagation, Interference and Diffraction of Light*. $6^{th}$ ed., Cambridge University Press (1980).

[32] Anzin V. B., Gorshunov B. P., Kozlov G. V., Volkov A. A., Lebedev S. P., Fedorov I. V., Schutzmann J., Renk K. F. *Measurement of electrodynamic parameters of superconducting films in far-infrared and submillimeter frequency ranges*. Appl. Supercond., vol. **1**, 467-478 (1993).

[33] Gorshunov B. P., Kozlov G. V., Volkov A. A., Lebedev S. P., Fedorov I. V., Prokhorov A. M., Makhov V. I., Schützmann J., Renk, K. F. *Measurement of electrodynamic parameters of superconducting films in the far-infrared and submillimeter frequency ranges*. Int. J. Infrared Milli Waves, vol. **14**, 683-702 (1993).

[34] Makise K., Mizokami Y., Nogami T., Sawada G., Asano T., Shinozaki B., Ichikawa F. *Estimations of superconducting fluctuation effects in amorphous MoRu and MoRe alloy thin films*, Mater. Res. Expr., vol. **5**, 096406 (2018).

[35] Mayadas A. F., Shatzkes M. *Electrical-resistivity model for polycrystalline films: the case of arbitrary reflection at external surfaces.*, Phys. Rev. B, vol. **1**, 1382 (1970).

[36] Sokolov A. V. *Optical Properties of Metals.* American Elsevier Publishing Company (1967).

[37] Dressel M., Grüner G. *Electrodynamics of Solids: Optical Properties of Electrons in Matter.* Cambridge University Press (2002).

[38] Sondheimer E. H. *The mean free path of electrons in metals.* Adv. Phys, vol. **50**, 499-537 (2001).

[39] Kittel C. *Introduction to Solid State Physics.* $8^{th}$ ed., Wiley (2004).

[40] Zimmermann W., Brandt E. H., Bauer M., Seider E., Genzel L. *Optical conductivity of BCS superconductors with arbitrary purity.* Physica C: Supercond., vol. **183**, 99-104 (1991).

[41] Glover III R. E., Tinkham M. *Conductivity of Superconducting Films for Photon Energies between 0.3 and 40 $kT_c$.* Phys. Rev., vol. **108**, 243 (1957).

[42] Palmer L. H., Tinkham M. *Far-Infrared Absorption in Thin Superconducting Lead Films.* Phys. Rev., vol. **165**, 588-595 (1968).

[43] Ginsberg D. M., Tinkham M. *Far Infrared Transmission through Superconducting Films.* Phys. Rev., vol. **118**, 990-1000 (1960).

[44] Richards P. L., Tinkham M. *Far-Infrared Energy Gap Measurements in Bulk Superconducting In, Sn, Hg, Ta, V, Pb, and Nb.* Phys. Rev., vol. **119**, 575-590 (1960).

[45] Tinkham M. *Introduction to Superconductivity.*, $2^{nd}$ ed., McGraw Hill (1996).

[46] Gorshunov,B. P., Volkov A. A., Prokhorov A. S., Spektor I.E. *Methods of terahertz-subterahertz BWO spectroscopy of conducting materials.* Phys. Solid State, vol. **50**, 2001-2012 (2008).

[47] Van Duzer T., Turner C. W. *Principles of superconductive devices and circuits.* $2^{nd}$ ed., Prentice Hall (1999).

[48] Miller P. B. *Surface impedance of superconductors.* Phys. Rev., vol. **118**, 928 (1960).

[49] Carrington A., Manzano F. *Magnetic penetration depth of $MgB_2$.* Physica C: Superconductivity, vol. 385, 205-214 (2003).

[50] De Gennes P. G. *Superconductivity of metals and alloys.* CRC press (2019).

[51] Maekawa S., Fukuyama H. *Localization effects in two-dimensional superconductors.* J. Phys. Soc. Japan, vol. **51**, 1380-1385 (1982).

[52] Finkel'shtein A. M. *Superconducting transition temperature in amorphous films.* JETP Lett., vol. **45**, 37-40 (1987); World Scientific Series in 20th Century Physics, vol. **11**, 288-291 (1996).

[53] Simonin J. *Surface term in the superconductive Ginzburg-Landau free energy: Application to thin films.* Phys. Rev. B, vol. **33**, 7830 (1986).

[54] Fàbrega L., Camón A., Fernández-Martínez I., Sesé J., Parra-Borderías M., Gil O., González-Arrabal R., Costa-Krümer J. L., Briones F. *Size and dimensionality effects in superconducting Mo thin films.* Supercond. Sci. Technol., vol. **24**, 075014 (1911).